IEEE Access
Multidisciplinary | Rapid Review | Open Access Journal

Received December 18, 2016, accepted January 26, 2017, date of publication February 8, 2017, date of current version March 28, 2017.

Digital Object Identifier 10.1109/ACCESS.2017.2664983

Model Predictive Control for Three-Phase Four-Leg Grid-Tied Inverters

QIHONG CHEN, (Member, IEEE), XIAORU LUO, LIYAN ZHANG, AND SHUHAI QUAN
School of Automation, Wuhan University of Technology, Wuhan 430070, China

Corresponding author: L. Zhang (zlywhut@whut.edu.cn)

This work was supported by the National Natural Science Foundation of China under Contract 61374050, Contract 61673306, and Contract 51477125.

ABSTRACT In order to improve the quality of the power injected into a grid, this paper presents a model predictive control strategy for three-phase four-leg grid-tied inverters. For the convenience of optimization, the discrete-time model of the inverter in which duty ratios are modeled as continuous control variables is investigated. A current tracking error oriented cost function is employed as a criterion to optimize duty ratios of the inverters. In order to eliminate the effects of sampling delay, a model predictive control with delay compensation method (MPC-DC) is proposed. Because there is a large amount of calculations in implementing predictive control algorithm, a double-CPU, namely FPGA plus DSP controller, is employed to implement parallel calculation, so as to reduce the computation time. Simulation and experimental results demonstrate the effectiveness of the proposed method.

INDEX TERMS Three-phase four-leg inverter, model predictive control (MPC), sampling delay, FPGA plus DSP.

I. INTRODUCTION

In recent years, distributed new energies, such as solar energy and wind energy, draw more and more attention from governments and researchers. As essential interfaces between distribution power sources and grids, inverters are used to inject high quality power into the grids. Control strategy is vital to energy efficiency and power quality of an inverter. Therefore, it is extremely significant to study control strategy of a grid tied inverter.

There are various topologies for grid-tied inverters. Due to the ability to supply unbalanced load and high utilization rate of DC voltage, three-phase four-leg topology is applied more and more widely in three-phase four-wire inverters [1]. High utilization rate of DC voltage means that inverters can output rated AC voltage with low input DC voltage. Many control strategies have been investigated for three-phase four-leg inverters. One of the most popular control strategies is 3D-SVPWM, which is in the mature stage [2].

Model predictive control (MPC) is a kind of model based optimal control strategy. It is widely used in process control area. Because of the ability of optimizing multi-variable, MPC has been investigated in more and more applications of power electronics. K. Shen *et al* [3] present a strategy of current model predictive control in dq rotating coordinates according to the characteristics of three-phase inverters. Hu *et al* [4]–[6] propose a model predictive direct power control (MPDPC) strategy for an inverter with unbalanced load and the grid used in a photovoltaic system. A two-step horizon prediction algorithm is developed to reduce switching frequency of a three-phase three-leg voltage source inverter [7]. Predictive control scheme is also used in an active power filter implemented by a four-leg voltage-source inverter [8], [9]. The dynamic response ability has been demonstrated by comparing with classical controllers. Rodriguez and Yaramasu [10]–[14] propose an algorithm of finite control set model predictive control (FCS-MPC) and investigate its application to voltage control of three-phase four-leg inverters [15]. FCS-MPC with two-step prediction has been presented to improve output voltage quality while reducing the number of switching state calculations and switching frequency [16].

However, the above MPC methods are based on finite control set, and state of each switch is fully on or off in one control period. As a result, current tracking error won't be as small as expected, and it's difficult to guarantee high quality of the power injected into the grid. Control precision and performance will be improved if duty ratio of each switch

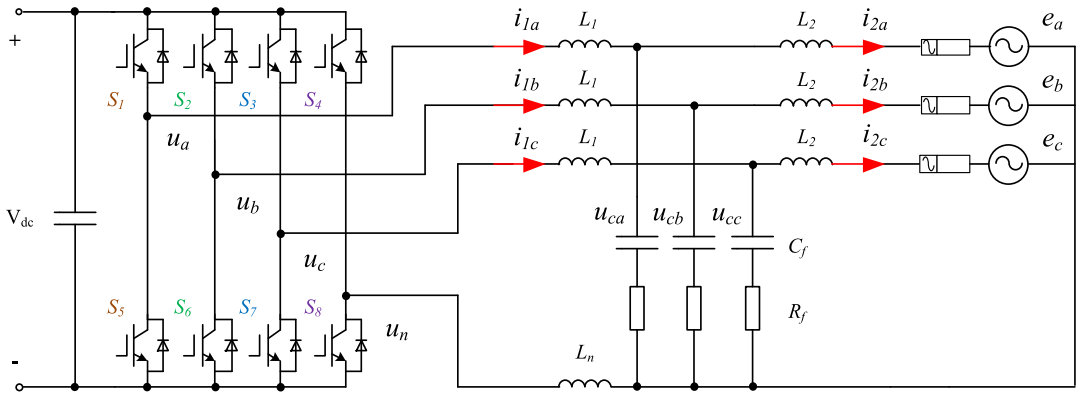

FIGURE 1. Configuration of a three-phase four-leg grid-tied inverter with *LCL* filter.

is controlled as a continuous variable in the range of [0, 1]. In this paper, model predictive control strategy is investigated to optimize duty ratio of each switch of three-phase four leg inverters.

The remaining contents are organized as follows. In Section II continuous and discrete-time models of the inverter, in which duty ratios are modeled as continuous control variables, are presented. This is followed by presenting model predictive control strategy in Section III. Section IV introduces simulation and experiment results. Finally, section V concludes this paper.

II. MODEL OF THE INVERTER

Configuration of the three-phase four-leg inverter with *LCL* filters is shown in Fig.1. Three damping resistances R_f are added to the filter circuit and serially connected to the capacitors C_f to eliminate resonance. As we can see, there are 8 power switches in the inverter, which are named as $S_1 \sim S_8$. Leg A, B, and C are connected to filter inductors L_1 of the corresponding phases, and inject power into the grid through serially connected inductors L_2, respectively. Leg N, namely the fourth leg, is connected to the *LCL* filter and grid through a neutral inductor L_n. V_{dc} is the input DC voltage. Three-phase current of inductor L_1 and the three-phase current injected into the grid are i_{1a}, i_{1b}, i_{1c}, i_{2a}, i_{2b}, and i_{2c}, respectively. To simplify analysis, voltage and current vectors are defined as:

$$\begin{cases} v_c = \begin{bmatrix} u_{ca} & u_{cb} & u_{cc} \end{bmatrix}^T \\ v = \begin{bmatrix} u_{an} & u_{bn} & u_{cn} \end{bmatrix}^T \\ e_g = \begin{bmatrix} e_a & e_b & e_c \end{bmatrix}^T \\ i_1 = \begin{bmatrix} i_{1a} & i_{1b} & i_{1c} \end{bmatrix}^T \\ i_2 = \begin{bmatrix} i_{2a} & i_{2b} & i_{2c} \end{bmatrix}^T \end{cases} \tag{1}$$

where e_a, e_b, e_c and u_{ca}, u_{cb}, u_{cc} are grid voltage and filter capacitor voltage of phase A, B, and C, respectively. u_{an}, u_{bn}, u_{cn} are voltage of leg A, B, and C related to leg N.

According to Kirchhoff law of voltage and current, mathematical model of the grid-tied inverter can be described as the following equations:

$$\begin{cases} L_{eq} \cdot \dfrac{d}{dt} i_1 + R_f C_f \cdot \dfrac{d}{dt} v_c = v - v_c \\ C_f \cdot \dfrac{d}{dt} v_c = i_1 - i_2 \\ R_f C_f \cdot \dfrac{d}{dt} v_c - L_2 \cdot \dfrac{d}{dt} i_2 = e_g - v_c \end{cases} \tag{2}$$

where

$$L_{eq} = \begin{pmatrix} L_1 + L_n & L_n & L_n \\ L_n & L_1 + L_n & L_n \\ L_n & L_n & L_1 + L_n \end{pmatrix}.$$

Let T_a, T_b, T_c, T_n denote duty ratios of upper switches of leg A, B, C and N, respectively. According to control principle of the inverter, duty ratio of lower switch of each leg is 1-T_i ($i = A, B, C$, and N). Then the following equations exist:

$$\begin{cases} u_{an} = (T_a - T_n) \cdot V_{dc} \\ u_{bn} = (T_b - T_n) \cdot V_{dc} \\ u_{cn} = (T_c - T_n) \cdot V_{dc} \end{cases} \tag{3}$$

Substituting (3) into (2), continuous model of the inverter can be written in state-space form as:

$$\begin{cases} \alpha \cdot \dot{x} = \beta \cdot x + \gamma \cdot u + \delta \cdot e_g \\ y = C \cdot x \end{cases} \tag{4}$$

where

$$x = \begin{pmatrix} i_1^T & v_c^T & i_2^T \end{pmatrix}^T, \quad e_g = \begin{pmatrix} e_a & e_b & e_c \end{pmatrix}^T,$$
$$y = \begin{pmatrix} i_{2a} & i_{2b} & i_{2c} \end{pmatrix}^T, \quad u = \begin{pmatrix} T_a & T_b & T_c & T_n \end{pmatrix}^T,$$
$$\alpha = \begin{pmatrix} L_{eq} & R_f C_f \cdot I_{3\times3} & O_{3\times3} \\ O_{3\times3} & C_f \cdot I_{3\times3} & O_{3\times3} \\ O_{3\times3} & R_f C_f \cdot I_{3\times3} & -L_2 \cdot I_{3\times3} \end{pmatrix},$$
$$\beta = \begin{pmatrix} O_{3\times3} & -I_{3\times3} & O_{3\times3} \\ I_{3\times3} & O_{3\times3} & -I_{3\times3} \\ O_{3\times3} & -I_{3\times3} & O_{3\times3} \end{pmatrix},$$
$$\gamma = \begin{pmatrix} V_{dc} & 0 & 0 & \\ 0 & V_{dc} & 0 & O_{4\times6} \\ 0 & 0 & V_{dc} & \\ -V_{dc} & -V_{dc} & -V_{dc} & \end{pmatrix}^T,$$

$$\delta = C^T = \begin{pmatrix} O_{3\times 6} & I_{3\times 3} \end{pmatrix}^T.$$

$I_{i\times i}$ and $O_{i\times j}$ are i-order identity matrices and i-row j-column null, respectively.

Multiplying α^{-1} at both sides of equations (4), the model can be rewritten as

$$\begin{cases} \dot{x} = A \cdot x + B \cdot u + D \cdot e_g \\ y = C \cdot x \end{cases} \tag{5}$$

where $A = \alpha^{-1} \times \beta$, $B = \alpha^{-1} \times \gamma$, and $D = \alpha^{-1} \times \delta$. Digital implementation of the predictive control requires discrete-time model. The continuous-time model (5) is discretized as:

$$\begin{cases} x(k+1) = G \cdot x(k) + H \cdot u(k) + W \cdot e_g(k) \\ y(k+1) = C \cdot x(k+1) \end{cases} \tag{6}$$

where $G = e^{AT_s}$, $H = \int_0^{T_s} e^{A\cdot t} \cdot B dt$, $W = \int_0^{T_s} e^{A\cdot t} \cdot D dt$, and T_s is the control period.

Prediction horizon P and control horizon M are two essential parameters in MPC. The prediction horizon determines how long into the future the controller predicts the behaviour of the inverter for computing an optimal control. The control horizon determines how long into the future the controller predicts the control variables. They are chosen to get a good tradeoff between performance and computation time.

State of instant $k+p$ can be predicted at current time k by using state space equation (6).

$$\begin{cases} x(k+p|k) = G^p \cdot x(k) + H \cdot \sum_{i=1}^{p} G^{i-1} \cdot u(k+i-1) \\ \qquad\qquad + W \cdot \sum_{j=1}^{p} G^{j-1} \cdot e_g(k+j-1) \\ y(k+p|k) = C \cdot x(k+p|k) \end{cases} \tag{7}$$

where $p = 1, \ldots, P$, and $\forall p > M$, $u(k+p-1) = e_g(k+p-1) = 0_{M\times 1}$.

Equation (7) can be written as:

$$\begin{cases} X(k) = \Phi * x(k) + \Psi * U(k) + \Gamma * E_g(k) \\ Y(k) = Cs * X(k) \end{cases} \tag{8}$$

where

$$X(k) = \begin{pmatrix} x(k+1|k) \\ \vdots \\ x(k+P|k) \end{pmatrix}_{P\times 1}, \quad \Phi = \begin{pmatrix} G \\ \vdots \\ G^P \end{pmatrix}_{P\times 1},$$

$$Y(k) = \begin{pmatrix} y(k+1|k) \\ \vdots \\ y(k+P|k) \end{pmatrix}_{P\times 1},$$

$$U(k) = \begin{pmatrix} u(k) \\ \vdots \\ u(k+M-1) \end{pmatrix}_{M\times 1},$$

$$E_g(k) = \begin{pmatrix} e_g(k) \\ \vdots \\ e_g(k+M-1) \end{pmatrix}_{M\times 1},$$

$$Cs = \begin{pmatrix} C & \cdots & 0 \\ \vdots & \ddots & \vdots \\ 0 & \cdots & C \end{pmatrix}_{P\times P},$$

$$\Psi = \begin{pmatrix} H & 0 & \cdots & 0 \\ G\cdot H & H & \cdots & 0 \\ \vdots & \vdots & \ddots & \vdots \\ G^{P-1}\cdot H & G^{P-2}\cdot H & \cdots & G^{P-M}\cdot H \end{pmatrix}_{P\times M},$$

$$\Gamma = \begin{pmatrix} W & 0 & \cdots & 0 \\ G\cdot W & W & \cdots & 0 \\ \vdots & \vdots & \ddots & \vdots \\ G^{P-1}\cdot W & G^{P-2}\cdot W & \cdots & G^{P-M}\cdot W \end{pmatrix}_{P\times M}.$$

III. PREDICTIVE CONTROL OF THE INVERTER

A. PREDICTIVE CONTROL STRATEGY

MPC is usually used to predict output trajectory of a process and compute a series of control actions that will minimize the error between the predicted trajectory and desired trajectory. A significant advantage of the MPC over other control schemes is its ability to deal with multi-variables.

Generally, the MPC control process consists of future states or output prediction, scrolling optimization, and control signal implementation. An important step is to set a cost function for optimizing. In this paper, the most important control objective is to minimize current tracking errors between desired output and real output of the inverter. As a result, the cost function is defined as the following.

$$\begin{aligned} J(k) = {} & q \cdot \sum_{i=1}^{P} [i_{2a}^*(k+i) - i_{2a}(k+i|k)]^2 \\ & + q \cdot \sum_{i=1}^{P} [i_{2b}^*(k+i) - i_{2b}(k+i|k)]^2 \\ & + q \cdot \sum_{i=1}^{P} [i_{2c}^*(k+i) - i_{2c}(k+i|k)]^2 \\ & + r \cdot \sum_{j=1}^{M} T_a(k+j-1)^2 + r \cdot \sum_{j=1}^{M} T_b(k+j-1)^2 \\ & + r \cdot \sum_{j=1}^{M} T_c(k+j-1)^2 + r \cdot \sum_{j=1}^{M} T_n(k+j-1)^2 \end{aligned} \tag{9}$$

where q and r are weighting factors of output error and control variable, respectively. $i_{2a}^*(k+i)$, $i_{2b}^*(k+i)$, and $i_{2c}^*(k+i)$ are desired output at instant $k+i$. $i_{2a}(k+i|k)$, $i_{2b}(k+i|k)$, and $i_{2c}(k+i|k)$ are predictive output of instant $k+i$. $T_a(k+j-1)$, $T_b(k+j-1)$, $T_c(k+j-1)$, and $T_n(k+j-1)$ are duty ratios of upper switches of leg A, B, C, and N at instant $k+j-1$, respectively.

In equation (9), there are two control objectives. As primary terms, the first three terms deal with tracking of output currents. Rests of the terms are used to smooth the control variable. Weighting factors are employed to prioritize the

objectives. Because the tracking errors of output currents are the primary terms, q is always greater than r.

The control objectives is to minimize cost function $J(k)$, which is expressed in vector form as:

$$\min J(k) = [Y^*(k) - Y(k)]^T \cdot Q \cdot [Y^*(k) - Y(k)] + U(k)^T \cdot R \cdot U(k) \tag{10}$$

where

$$\begin{aligned} Y^*(k) &= \begin{pmatrix} y^*(k+1) & \cdots & y^*(k+P) \end{pmatrix}^T_{P\times 1}, \\ U(k) &= \begin{pmatrix} u(k) & \cdots & u(k+M-1) \end{pmatrix}^T_{M\times 1}, \\ Q &= diag(q \ldots q), \quad R = diag(r \ldots r), \\ y^*(k+i) &= \begin{pmatrix} i^*_{2a}(k+i) & i^*_{2b}(k+i) & i^*_{2c}(k+i) \end{pmatrix}^T, \\ y(k+i|k) &= C \cdot x(k+p|k) \\ &= \begin{pmatrix} i_{2a}(k+i|k) & i_{2b}(k+i|k) & i_{2c}(k+i|k) \end{pmatrix}^T, \end{aligned}$$

and $i = 1, \ldots, P$.

Substituting (8) into (10), and let derivative of the cost function $\frac{\partial J(k)}{\partial U(k)} = 0$, control variable can be expressed as:

$$U(k) = (\Psi^T C_s^T Q C_s \Gamma - R)^{-1} \times \Psi^T C_s^T Q \times [Y^*(k) - C_s\Phi \cdot x(k) - C_s\Gamma \cdot E_g(k)] \tag{11}$$

Let $\lambda = \xi \cdot (\Psi^T C_s^T Q C_s \Psi - R)^{-1} \cdot \Psi^T C_s^T Q$, $\xi = [1\ 0\ \ldots\ 0]_{1\times M}$. Equation (11) can be rewritten as:

$$u(k) = \lambda_1 \cdot Y^*(k) - \lambda_2 \cdot x(k) - \lambda_3 \cdot E_g(k) \tag{12}$$

where $\lambda_1 = \lambda$, $\lambda_2 = \lambda \cdot C_s\Phi$, $\lambda_3 = \lambda \cdot C_s\Gamma$. Therefore, Duty ratios of switches of the inverter can be calculated according to expression (12).

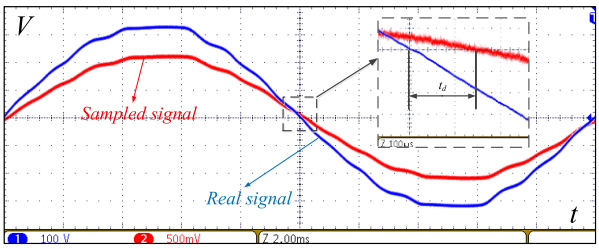

FIGURE 2. Sampling delay of real signal.

B. COMPENSATION OF SAMPLING DELAY

In order to optimize control variable, it's necessary to sample output current and voltage of each phase. In practical application, the current and voltage are transformed into analog signals by Hall sensors, and are sampled by a digital signal processor (DSP) after filtering. There is time delay in the process of signal processing and acquiring, which have a negative effect on accuracy of MPC. Sampling delay of real signal gotten through oscilloscope is shown in Fig. 2.

t_d is the time delay caused by signal processing and acquiring. It is noticed that sampling delay of the inverter is about 150μs. It means that the signal sampled by the controller at instant k is output signal of the inverter at instant $k-3$. As a result, the state variable obtained by the controller at instant k is $x(k-3)$, not $x(k)$.

In order to enhance control performance, a MPC with delay compensation (MPC-DC) is presented to eliminate the effect of sampling delay.

The time delay is about triple of control period, we can rewrite the prediction expression (7) as the following equation.

$$\tilde{x}(k) = G^3 \cdot x(k-3) + H \cdot \sum_{i=1}^{3} G^{i-1} \cdot u(k+i-4) + W \cdot \sum_{j=1}^{3} G^{j-1} \cdot e_g(k+j-4) \tag{13}$$

where $\tilde{x}(k)$ is the estimation value of $x(k)$. In expression (12), $x(k)$ is substituted by $\tilde{x}(k)$.

$$u(k) = \lambda_1 \cdot Y^*(k) - \lambda_2 \cdot \tilde{x}(k) - \lambda_3 \cdot E_g(k) \tag{14}$$

Parameters q, r, P, *and* M can be given. Matrixes λ_1, λ_2 and λ_3, are constant and can be calculated directly. Therefore, All essential conditions for solving $u(k)$ are known, the proposed MPC-DC can be realized through software.

C. IMPLEMENTATIONS

This section primarily discusses the implementation scheme of MPC-DC strategy. There are primarily two schemes for MPC-DC of an inverter:

(1) DSP-based control scheme. This is a traditional method, but it's difficult to guarantee calculation speed.
(2) FPGA (Field Programmable Gate Array) plus DSP hybrid architecture. This scheme is designed for MPC-DC strategy specially.

Because control period is usually dozens of microseconds, the inverter has a strict requirement about calculation speed. However, MPC-DC involves a large number of matrix calculations. For scheme (1), DSP has abundant of hardware interface, but it is hard to meet the requirement about computing speed. Contrarily, an FPGA has powerful parallel operation capacity. As a result, dual CPU hybrid architecture, namely DSP plus FPGA are employed to design the controller. The implementation diagram is shown in Fig. 3.

Parallel data communication is deployed between DSP and FPGA. They can exchange data through a virtual double port RAM (DPRAM) built in FPGA. The output current, grid voltage, current of L_1 and voltage of C_f are sampled by DSP and transferred to FPGA. In succession, FPFA calculates duty ratios of the switches according to equation (11), and transfers the computing results to DSP. Finally, DSP generates PWM signals based on the received duty ratios and control the IGBTs.

In the controller, MPC-DC is programmed in FPGA as an individual module. The MPC-DC module reads data from DPRAM, and gets angles of phase A, B, and C according to phase-locked loop (PLL). Reference $Y^*(k)$ can be calculated by using the phase angles. Control variable $u(k)$ is

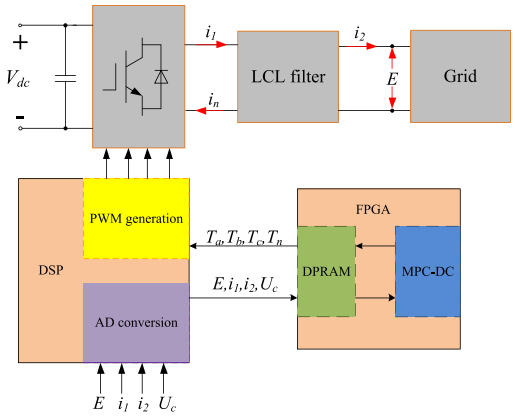

FIGURE 3. Implementation diagram based on FPGA plus DSP hybrid architecture.

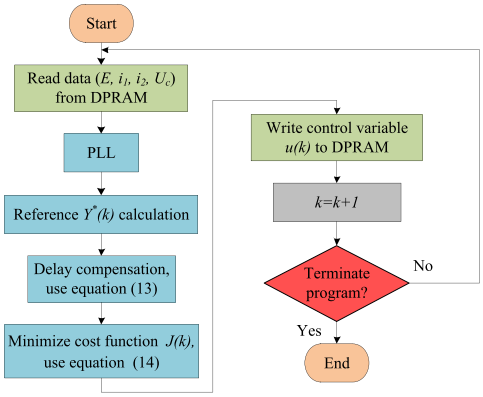

FIGURE 4. Flow chart of model predictive control strategy.

computed after delay compensation. Finally, MPC-DC writes duty ratios to DPRAM, and then waits for next step. Detail flow chart is shown in Fig. 4.

IV. SIMULATION AND EXPERIMENT

In this section, effectiveness of the proposed MPC-DC strategy is verified by simulation in MATLAB/ Simulink and experiment of inverter prototype. The parameters used in the simulation and experiment are given in Table 1.

A. SIMULATION

The three-phase four-leg grid-connected inverter is shown in Fig. 1, and a predictive controller was implemented by MATLAB/Simulink based on the parameters given in Table 1.

Prediction horizon and control horizon directly affect not only the amount of calculation, but also rapidity and stability of the inverter. A MPC with smaller P and larger M has greater rapidity and worse stability. On the contrary, larger P and smaller M will cause worse rapidity and greater stability. P and M were set as 2 to gain good tradeoff between rapidity and stability.

The weighting factors, named q and r, have close relationship with tracking error and power quality. The guidelines proposed in [17] were used to determine weighting factors.

TABLE 1. Parameters of the inverter.

Variable	Description	Value
V_{dc}	DC-link Voltage	700V
P_e	Rated Power	10kW
I_e	Rated Current	15A
V_g	Grid RMS Voltage	220V
f_n	Grid Frequency	50Hz
T_s	Control period	50μs
L_1	Filter Inductance	3.2mH
L_2	Filter Inductance	1.2mH
L_n	Filter Inductance	1.2mH
C	Filter Capacitance	5μF
R	Filter Resistance	22Ω

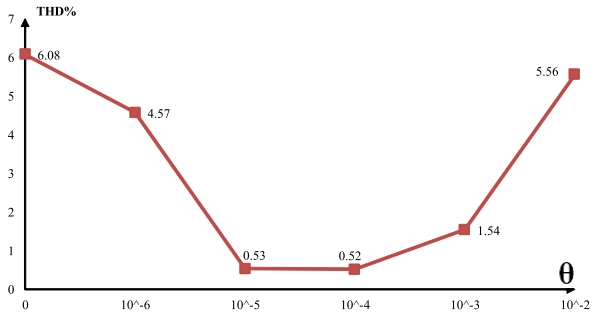

FIGURE 5. Relationship of current THD and θ.

Let $\theta = r/q$. In the cost function, there is a growing influence of control variables with the increasing θ. However, if θ is too small, there are weak optimization effects on control variables, and the stability of the inverter will become worse. If θ is too large, we can't guarantee minimum tracking errors. Therefore, q and r should be chosen reasonably. The relationship of current THD and θ is shown in Fig. 5.

In Fig. 5, θ gradually increases from zero to 10^{-2}, but THD of the output current doesn't change monotonically. When $0 < \theta < 10^{-5}$, THD decreases from 6.08% to 0.53% rapidly. When $10^{-5} \leq \theta \leq 10^{-4}$, THD is nearly constant. When $10^{-4} < \theta \leq 10^{-2}$, on the contrary, THD increases from 0.52% to 5.56% step by step. Hence, the ratio of weighting factors r and q should be in the range $[10^{-5}, 10^{-4}]$. According to this rule, θ is set as 10^{-5}. Correspondently, r and q were set as 0.1 and 10000, respectively.

The simulation results of MPC, MPC-DC and PI controller are shown in Fig. 6. The PI parameters (p and i) were set as 40 and 2, respectively.

In the simulations, the inverter operated at rated power, and the reference current of each phase was 15A. As shown in Fig. 6, Fig. 7, and Fig. 8, there are significant differences among three methods. Tracking errors of MPC-DC and PI are less than that of MPC. The current tracking error of MPC is 2.02A, which is almost one- sixth of the reference current. However, MPC-DC injects higher quality power into the grid.

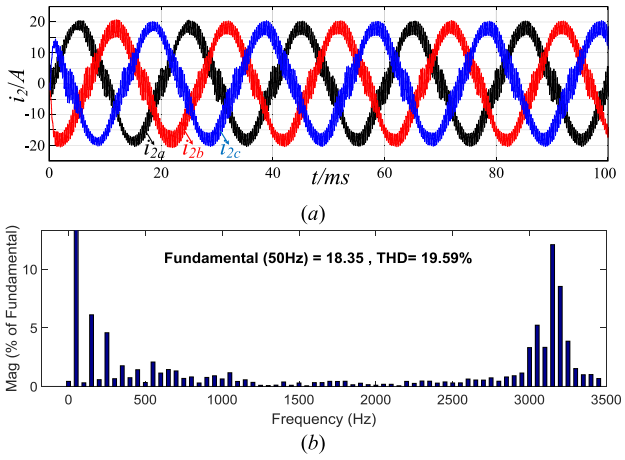

FIGURE 6. Simulation results of MPC: (*a*) Output current. (*b*) FFT analysis.

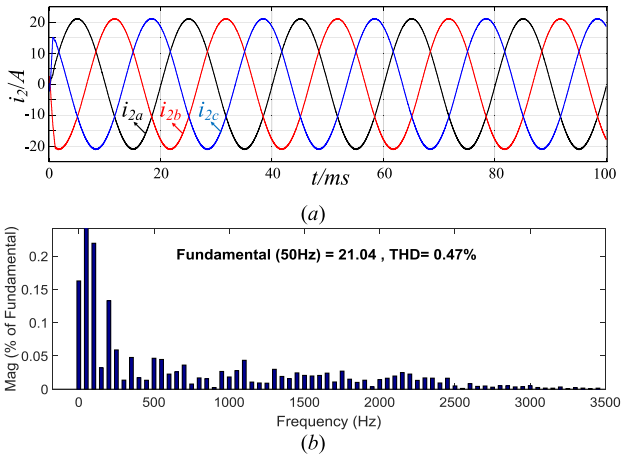

FIGURE 7. Simulation results of MPC-DC: (*a*) Output current. (*b*) FFT analysis.

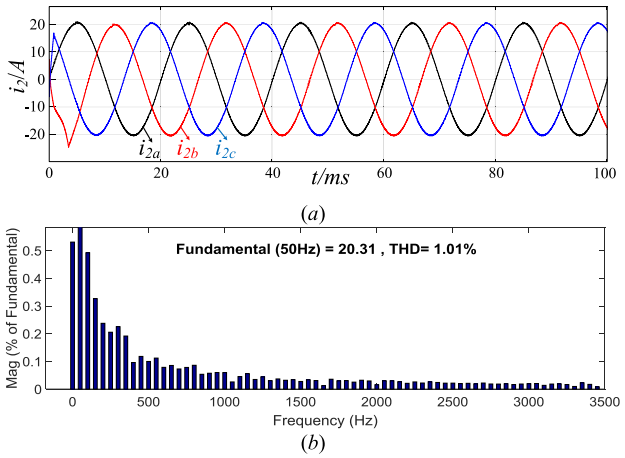

FIGURE 8. Simulation results of PI controller: (*a*) Output current. (*b*) FFT analysis.

It means that the proposed method of delay compensation is effective.

In [13], a method of FCS-MPC with two-step prediction was presented. Current THD of this method is more than 2%,

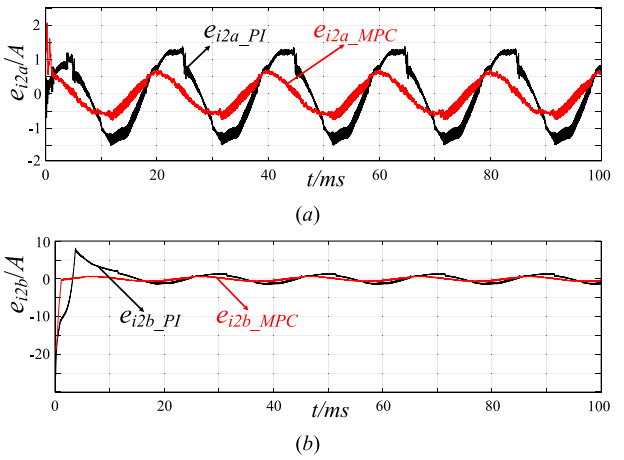

FIGURE 9. Current tracking errors: (*a*) Phase A. (*b*) Phase B.

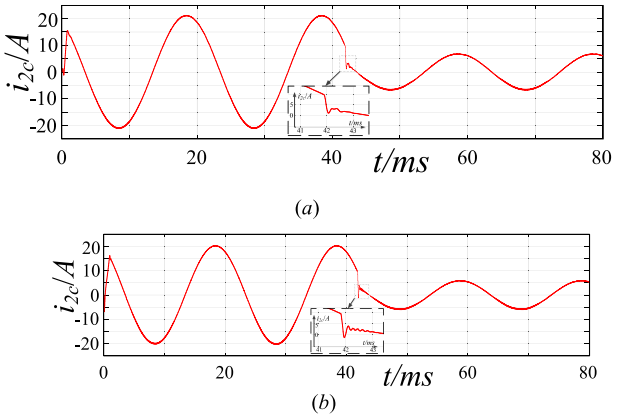

FIGURE 10. Output current of phase C with a varied amplitude reference current: (*a*) MPC-DC. (*b*) PI controller.

which is higher than that of MPC-DC, approximately 0.5%. It shows superiority of MPC-DC.

Compared with PI control, output current of MPC-DC is obviously smoother. What's more, MPC-DC reduces THD by 0.54% and increases the RMS (Root Mean Square) of fundamental by 0.5A compared with PI control. Output currents of MPC-DC are closer to expected currents. Hence, the MPC-DC strategy provides higher quality power.

Current tracking errors of Phase A of MPC-DC and PI control are denoted as e_{i2a_MPC} and e_{i2a_PI}, respectively. Similarly, current tracking errors of Phase B of MPC-DC and PI control are denoted as e_{i2b_MPC} and e_{i2b_PI}, respectively. Current tracking errors of phase A and B are shown in Fig. 9.

Current tracking error is the difference between output current and expected current. In Fig. 9 (*a*), current tracking error of phase A of PI control (e_{i2a_PI}) is approximately sinusoidal, and the maxium value is 1.5A, which is bigger than that of MPC, 0.6A. As a result, steady state performance of MPC is better than PI control.

Tracking errors in Fig. 9 (*b*) is much bigger than that in Fig. 9 (a) at beginning. The reason is that the inverter was tied to the grid when grid voltage of phase A was zero. Settling time of MPC and PI control, t_{s_MPC} and t_{s_PI}, are 1ms and

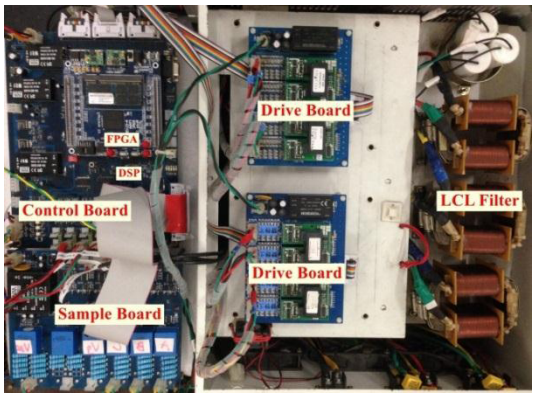

FIGURE 11. Photo of the grid tied inverter.

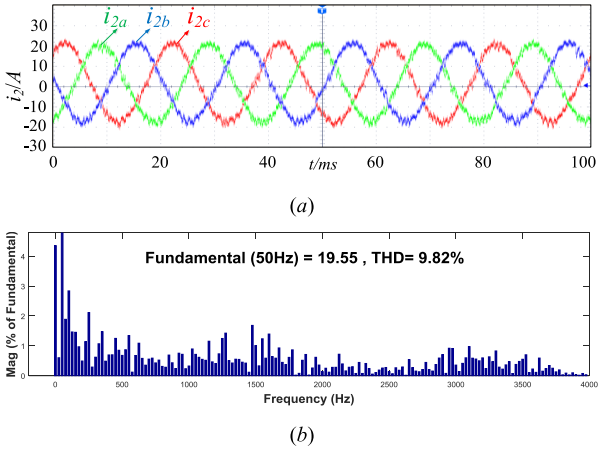

FIGURE 12. Experimental results of MPC: (*a*) Output current. (*b*) FFT analysis.

14ms, respectively. Dynamic performnace of MPC is better than PI control. Overshoot of MPC is also much smaller than that of PI control, 8A.

To get better comparison of dynamic perforamce of MPC-DC and PI, we changed amplitude of reference currents, and the output current of phase C is shown in Fig. 10.

Tracking time of MPC-DC is 0.7ms , which is much shorter than that of PI controller, about 1.2ms. Moreover, overshoot of MPC-DC is only 1.8A, which is much smaller than overshoot of PI, almost 5A. It demonstrates that the MPC-DC has better dynamic performnace than PI controller.

In conclusion, the MPC-DC strategy has smaller steady-state error, less overshoot and faster response speed.

B. EXPERIMENT

To further validate the feasibility of MPC strategy, a three-phase four-leg grid-tied inverter was set up according to Fig. 1 and Table 1. Infineon IGBTs were employed. A FPGA plus DSP control board was used to implement the real-time control algorithm. The type of FPGA is EP4CE115F23I7 produced by Altera, and the DSP is TMS320F28335 produced by TI. A sampling board with three-channel AC voltage sampling, single-channel DC voltage sampling and three-channel AC current sampling was connected the FPGA plus DSP control board. Four IGBT driver modules were used to

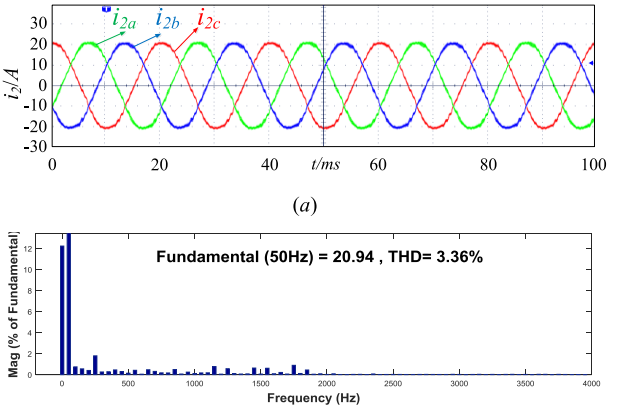

FIGURE 13. Experimental results of MPC-DC: (*a*) Output current. (*b*) FFT analysis.

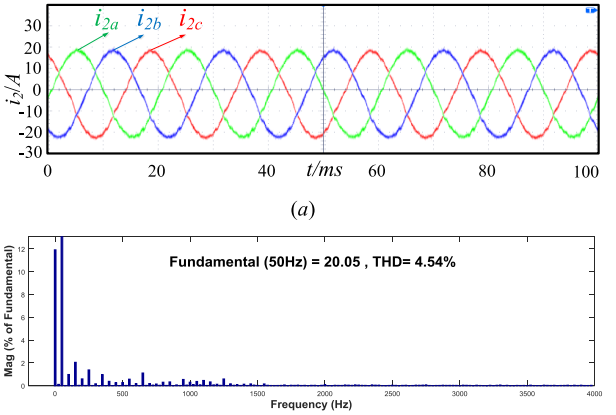

FIGURE 14. Experimental results of PI controller: (*a*) Output current. (*b*) FFT analysis.

receive the PWM signals from DSP, and drive the IGBTs. The inverter is shown as Fig. 11.

After assembling of the inverter, it is found that calculation time of MPC in FPGA is 8μs, and the communication time between FPGA and DSP is less than 6μs. Therefore, total operating time of each control period is less than 20μs, which satisfies the requirement about speed of the three-phase four-leg inverter.

The PI parameters used in experiment were set as 24 and 1.2, respctively. These parameters have been used in an inverter prototype.

Fig. 12, Fig. 13 and Fig. 14 are the experimental results of three strategies, respectively. Compared with MPC, MPC-DC reduces THD by 6.46%, and increases the RMS of fundamental by 1A. The output current of MPC strategy contains a large number of harmonics, even more than PI control strategy. Therefore, sampling delay compensation method has significant effect on inverter performance.

The experimental result of MPC-DC and PI control are very similar to simulation results. Compared with PI control, MPC-DC strategy decreases THD by 1.18%, and increases

the RMS of fundamental by 0.64A. The experimental results show that MPC-DC strategy has better performance than PI controller. Compared with THD of FCS-MPC, which was 6%[14], MPC-DC is also better.

The experimental results are similar to simulation results, but the simulation results are better. The reason is that the grid voltage is sinusoidal and constant in simulation, but the inverter is connected to the real grid, which has lots of disturbance. Nonetheless, the experimental results have demonstrated that the proposed MPC-DC strategy is feasible and effective.

V. CONCLUSIONS

A model predictive control strategy has been proposed for a three-phase four-leg grid-tied inverter with output *LCL* filters. Firstly, a novel discrete-time state-space predictive model, in which duty ratios are control variables, is presented. In succession, in order to solve the sampling delay problem, the MPC-DC strategy is investigated. A hardware scheme based on FPGA plus DSP hybrid architecture is employed to implement the proposed MPC-DC strategy. Finally, simulation and experiment results are provided to demonstrate MPC-DC strategy. According to the comparison between PI control and MPC-DC, it is found that MPC-DC can significantly improve steady state and dynamic performance of the inverter. We will focus on constrained model predictive control to further improve performance of an inverter in the future.

REFERENCES

[1] X. Li and Z. Deng, "Analysis and simplification of three-dimensional space vector PWM for three-phase four-leg inverters," *IEEE Trans. Ind. Electron.*, vol. 58, no. 2, pp. 450–464, Feb. 2011.

[2] Q. Chen and J. Wang, "A control method of three-phase four-leg grid-tied inverter," China Patent CN104 578 878A, Apr. 25, 2015.

[3] K. Shen and J. Zhang, "Model predictive control of three-phase three-wire voltage source inverters," *Trans. China Electrotech. Soc.*, vol. 28, no. 12, pp. 283–289, Dec. 2013.

[4] J. Hu, J. Zhu, and D. G. Dorrell, "Model predictive control of grid-connected inverters for PV systems with flexible power regulation and switching frequency reduction," *IEEE Trans. Ind. Appl.*, vol. 51, no. 1, pp. 587–594, Jan. 2015.

[5] Y. Zhang, W. Xie, and Z. Li, "Model predictive direct power control of a PWM rectifier with duty cycle optimization," *IEEE Trans. Power Electron.*, vol. 28, no. 11, pp. 5343–5351, Nov. 2013.

[6] Y. Zhang, W. Xie, and Z. Li, "Model predictive direct power conrol of PWM rectifiers under unbalanced network conditions," *IEEE Trans. Ind. Electron.*, vol. 62, no. 7, pp. 4011–4022, Jul. 2015.

[7] P. Cortes *et al.*, "Classical methods and model predictive control of three-phase inverter with output LC filter for UPS applications," *IEEE Trans. Ind. Electron.*, vol. 56, no. 6, pp. 1875–1883, Jun. 2009.

[8] P. Acuna, L. Moran, M. Rivera, J. Dixon, and J. Rodriguez, "Improved active power filter performance for renewable power generation systems," *IEEE Trans. Ind. Electron.*, vol. 29, no. 2, pp. 687–694, Feb. 2014.

[9] P. Acuna, L. Moran, M. Rivera, J. Rodriguez, and J. Dixon, "Improved active power filter performance for distribution systems with renewable generation," in *Proc. 38th Annu. Conf. IEEE Ind. Electron. Soc.*, Montreal, Canada, Dec. 2012, pp. 1344–1349.

[10] J. Rodriguez, B. Wu, M. Rivera, A. Wilson, V. Yaramasu, and C. Rojas, "Model predictive control of three-phase four-leg neutral-point-clamped inverters," in *Proc. Int. Power Electron. Conf.*, Sapporo, Japan, Apr. 2010, pp. 3112–3116.

[11] J. Rodriguez, B. M. Wu Rivera, and V. Yaramasu, "Predictive current control of three-phase two-level four-leg inverter," in *Proc. 13th Int. Power Electron. Motion Control Conf.*, Novi Sad, Serbia, Sep. 2010, pp. T3-106–T3-110.

[12] M. Rivera, V. Yaramasu, J. Rodriguez, and B. Wu, "Model predictive current control of two-level four-leg inverters—Part II: Experimental implementation and validation," *IEEE Trans. Power Electron.*, vol. 28, no. 7, pp. 3469–3478, Jul. 2013.

[13] V. Yaramasul, B. Wul, M. Rivera, and J. Rodriguez, "Enhanced model predictive voltage control of four-leg inverters with switching frequency reduction for standalone power systems," in *Proc. 17th Int. Power Electron. Motion Control Conf.*, Novi Sad, Serbia, Sep. 2014, pp. DS2c.6-1–DS2c.6-5.

[14] M. Rivera and V. Yaramasu, "Digital predictive current control of a three-phase four-leg inverter," *IEEE Trans. Ind. Electron.*, vol. 60, no. 11, pp. 4903–4912, Nov. 2013.

[15] Z. Liu, J. Liu, and J. Li, "Modeling, analysis and mitigation of load neutral point voltage for three-phase four-leg inverter," *IEEE Trans. Ind. Electron.*, vol. 60, no. 5, pp. 2010–2021, May 2013.

[16] V. Yaramasu, M. Rivera, and M. Narimani, "Model predictive approach for a simple and effective load voltage control of four-leg inverter with an output LC filter," *IEEE Trans. Ind. Electron.*, vol. 61, no. 10, pp. 5259–5270, Oct. 2014.

[17] P. Cortés, S. Kouro, B. La Rocca, R. Vargas, and J. Rodríguez, "Guideline for weighting factors design in model predictive control of power converters and drives," in *Proc. IEEE Int. Conf. Ind. Technol.*, Busan, Korea, May 2009, pp. 1–7.

[18] F. Liu, X. Cha, and S. Duan, "The parameters design and research of three-phase grid-connected inverters with an output LCL filter," *Trans. China Electrotech. Soc.*, vol. 25, no. 3, pp. 110–116, Mar. 2010.

[19] X. Wei, "The research of of three-phase grid- connected inverters with an output LCL filter," M.S. thesis, Dept. Electron. Eng., Nanjing Univ. Aero. and Astr., Nanjing, China, 2011.

QIHONG CHEN (M'08) received the Ph.D. degree in control science and engineering from Southeast University, Nanjing, China, in 2003. He is currently a Professor with the Wuhan University of Technology, Wuhan, China. His current research interests include grid tied inverters and predictive control.

XIAORU LUO received the B.S. degree from the Wuhan University of Technology, Wuhan, China, in 2014, where he is currently pursuing the M.S. degree. His research interests include model predictive control for inverters.

LIYAN ZHANG received the Ph.D. degree in control science and engineering from Zhejiang University, Hangzhou, China, in 2004. He is currently a Professor with the Wuhan University of Technology, Wuhan, China. His current research interests include predictive control, and modeling and control of hybrid electric vehicles.

SHUHAI QUAN received the Ph.D. degree in mechanical engineering from the Wuhan University of Technology, Wuhan, China, in 2002. He is currently a Professor with the Wuhan University of Technology. His current research interests include new energy power conversion and access technology.